Research article

Effect of sucrose-based carbon foams as negative electrode additive on the performance of lead-acid batteries under high-rate partial-state-of-charge condition

Fazhi Xie [a,b,*], Yujia Ma [a], Meng Zhang [a], Shaohua Yang [c], Yuan Dai [b], Liang Fang [c], Yonggang Shao [c]

[a] School of Materials and Chemical Engineering, Anhui Jianzhu University, Hefei 230601, China
[b] School of Environment and Energy Engineering, Anhui Jianzhu University, Hefei 230601, China
[c] Anhui Accord Science and Technology Co, LTD, Huangshan 242700, China

ARTICLE INFO

ABSTRACT

Lead-acid batteries are noted for simple maintenance, long lifespan, stable quality, and high reliability, widely used in the field of energy storage. However, during the use of lead-acid batteries, the negative electrode is prone to irreversible sulfation, failing to meet the requirements of new applications such as maintenance-free hybrid vehicles and solar energy storage. In this study, in order to overcome the sulfation problem and improve the cycle life of lead-acid batteries, active carbon (AC) was selected as a foaming agent and foam fixing agent, and carbon foams (CF) with layered porous structure was prepared by mixing with molten sucrose. Sucrose as raw material is green and cheap, and the material preparation process is simple. The prepared CF material was then added as an additive to the negative electrode plate, and the electrochemical performance of the electrode plate and the battery was studied. The results proved that the addition of CF could effectively inhibit the sulfate formation of the negative electrode plate, with the 1.0 % CF negative electrode plate showing the best electrochemical performance. Specifically, according to the result of battery cycle testing, the simulated battery with CF had a cycle life of 3642 times, which was 2.87 times that of the blank group and 2.39 times of the AC group. Meanwhile, rate testing showed that the simulated battery with CF could maintain a high capacity even under high-rate discharge conditions.

1. Introduction

The lead-acid battery, first invented by a French physicist and chemist named Gaston Planté in 1859, has since undergone more than 160 years of development. It is one of the most widely used rechargeable batteries, which are mainly used in automobiles, communications, solar energy, and power plants [1–4]. Lead-acid batteries suffer from short cycle life and low discharge capacity at low temperature [5]. Irreversible sulfation of the negative electrode of lead-acid batteries at HRPSoC is one of the main reasons for the short cycle life of the batteries. While the lead-acid battery is discharged in the HRPSoC state, fine $PbSO_4$ crystals will be formed on the surface of the negative electrode plate, and these fine crystals are easy to dissolve, with some of the resulting Pb^{2+} continuing to

---

* Corresponding author.
  E-mail address: fzxie@ahjzu.edu.cn (F. Xie).

participate in the subsequent reaction, while the other part of Pb^{2+} forms large $PbSO_4$ crystals of low solubility through the recrystallisation process [6]. These large $PbSO_4$ crystals cannot be completely converted into sponge lead, resulting in partial loss of negative active material (NAM). At the same time, $PbSO_4$ gradually accumulates on the negative electrode plate, forming an insulating layer that hinders the diffusion of electrolyte into the plate, thus affecting the battery's cycle life. To address the problem of irreversible sulfation of the negative electrode, M. Shiomi et al. [7] added carbon materials to the negative electrode plate, finding that high surface area carbon can form a conductive network, hence promoting high-rate charging of the battery while inhibiting negative electrode sulfate formation. Carbon materials are favored by most of the researchers such as active carbon [8], carbon black [9], graphite [10], biomass charcoal [11] have been incorporated as additives in the negative electrode plate.

The incorporation of carbon materials can effectively prevent sulfation of lead-acid batteries and improve the charge acceptance and cycle life of the batteries. A. Banerjee et al. [12] added single-wall carbon nanotube to lead-acid batteries and a very small amount was effective in inhibiting sulfation. Carbon can form a conductive network in NAM and increase the conductivity of NAM [13–16]. It can also increase the active surface area and improve the charge acceptance ability of the battery. S.W. Swogger et al. [17] used discrete carbon nanotubes as negative electrode additives in lead-acid batteries to improve battery capacity and charge acceptance. D. Pavlov et al. [18] found that the reduction electrochemical reaction of lead ions can be carried out simultaneously on the surface of lead and carbon particles, which improving the reversibility of the battery's charging/discharging process, increasing charging efficiency, while slowing down the sulfate formation on the negative electrode plate. Carbon can provide more reactive sites for H_2SO_4, which is conducive to the full reaction of the electrolyte into the interior of the negative plate [19]. In this way, the small-sized $PbSO_4$ crystals can be dispersed throughout the plate, preventing the accumulation of a passivation layer on the surface and greatly inhibiting the sulfation of the negative plate [20]. Therefore, adding carbon materials to the negative electrode plate can effectively increase the utilization of active materials and improve the conversion efficiency from $PbSO_4$ to Pb. In addition, carbon materials also increase battery capacity and act as supercapacitors in NAM [21]. P.T. Moseley et al. [22] proposed that carbon materials can also form a double layer capacitance at the negative electrode, which improves the charging and discharging capabilities of batteries at high rates. A. Jaiswal et al. [23] showed that the addition of carbon increases the Faraday charge of NAM and high specific surface area carbon also increases the capacitive charge.

In this study, we prepared porous CF material by using AC foaming technology, and systematically studied its effectiveness as an additive to the battery's negative electrode. We also described the electrochemical performance of lead-acid batteries through cyclic voltammetry (CV), linear sweep voltammetry (LSV) and electrochemical impedance spectroscopy (EIS), as well as by charging and discharging cycles of the batteries in the same electrolyte solution. The results showed that the CF-added batteries could effectively prevent the sulfation of the negative plate, significantly improve the electrochemical performance, improve the charge/discharge cycle, and increase the cycle life of the batteries. Among the batteries with different CF contents, 1.0 % CF has the best electrochemical performance and the longest battery cycle life.

2. Experiment

2.1. Preparation of CF

To prepare CF, a mixture was prepared by uniformly mixing 10 g of sucrose and AC powder with a weight ratio of 0.05. The mixture was then heated in a beaker at 170 °C until the sucrose was completely melted. Afterward, the melted sucrose was thoroughly dispersed with the AC powder using a glass rod. The sucrose-AC powder mixture was heated at 130 °C for 36 h to allow foaming and shaping, and then dried in an oven at 200 °C for 3 h. The dried material was heated in a nitrogen protected environment at 900 °C for 2 h to carbonize it. It was naturally cooled to room temperature and the sample was removed and ground to obtain CF [24].

2.2. Negative plate preparation

The preparation of the negative electrode plate involved the uniform mixing and dispersion of lead oxide powder (98.49 wt%), $BaSO_4$ (0.8 wt%), short fibers (0.06 wt%), lignin (0.1 wt%), humic acid (0.25 wt%), acetylene black (0.3 wt%) and CF material. An appropriate volume of water and dilute sulfuric acid (1.4 g/ml, the mass ratio of sulfuric acid to lead powder is 0.075:1) were added to the mixture, followed by mechanical stirring, until a paste-like consistency was achieved. The resulting paste was then uniformly applied onto a grid, compacted, and drenched with acid for 15–20 s. Subsequently, the plate was subjected to curing and drying under relative humidity and temperature conditions. The curing and drying conditions are as follows: at about 95 % relative humidity, first, overnight at 40 °C, then cured at 45, 55, 65, 75 °C for 4h and finally at 80 °C for 4h.

2.3. Material characterizations

To determine the composition and morphology of the material, characterization tests and analyses were conducted. Scanning electron microscope (SEM, Hitachi HITACHI SU8010) and energy dispersive spectrometer (EDS, X-max N HORIBA) were used to observe the microscopic morphology and elemental composition of the materials, and the crystal structure and composition of CF materials were characterized and analyzed using instruments such as X-ray diffraction (XRD, Bruker D8 Advance), Fourier transform infrared spectroscopy (FTIR. Nicolet 6700 FT-IR) and other instruments for characterization and analysis. The elemental species and chemical states of the materials were analyzed by X-ray photoelectron spectroscopy (XPS, Thermo Fisher Scientific K-Alpha, USA). Raman spectroscopy (Renishaw inVia) was used to analyze the molecular structure of substances. N_2 adsorption-desorption isotherms

were measured by an Autosurb iQ (micromeritics ASAP 2460) instrument and used to analyze the specific surface area and porosity of the material.

2.4. Electrochemical measurements

In order to study the performance of negative plates with different contents of CF, four negative plates (0.5 % CF, 1.0 % CF, 1.5 % CF and 2.0 % CF) were prepared as the experimental group, 1.0 % AC as the control group, and the negative plate without any additives as the blank group. The effect of CF additives on the electrode capacitance was analyzed by CV, the hydrogen evolution performance of the electrode plate by LSV, and EIS is used to analyze the change of electrode impedance. The electrochemical measurements were carried out by means of an electrochemical workstation using a three-electrode system with an electrolyte of 1.23 g/ml H_2SO_4 solution, a homemade negative electrode plate as the working electrode, and mercury sulfate electrode and platinum electrode as the reference electrode and auxiliary electrode, respectively. The CV was tested with a scan rate of 0.01 V/s over a voltage range of −1.4 V–0.4 V. The voltage range of LSV was −1.1 V–0.2 V with a scan rate of 5 mV/s. The EIS was carried out over a range of 100 kHz to 0.1 Hz, with an amplitude of 5 mV, and the resulting EIS curves were fitted using Zview [25].

2.5. Battery performance measurements

The simulated test battery used in this study was a closed lead-acid battery with a voltage of 2.0 V. It consisted of one negative plate and two positive plates assembled together, separated by a 3 mm thick AGM separator. The battery was immersed in an aqueous 1.23 g/cm³ H_2SO_4 solution and then sealed in a battery container with a pressure between 15 and 30 kPa. To further investigate the role of CF additives in batteries, the cycle life and multiplier test of batteries at HRPSoC were tested. Additionally, the assembled simulated battery underwent rated capacity testing to investigate its discharge capacity. The cycle life test of the battery at HRPSoC was performed as follows: first, charge at 0.1 C to a cutoff voltage of 2.4 V, then charge at 2.4 V for 12 h and set aside for 10 min, then discharge at 1 C to 50 % SoC and set aside for 10 min, and lastly, perform a high rate charging/discharging cycle, charging at 2 C for 60 s and set aside for 10 s, and discharging at 2 C for 60 s and set aside for 10 s until the discharge cutoff voltage of 1.7 V. The multiplier test was performed by charging at 0.1 C constant current to 2.4 V for 30 s, then charging at 2.4 V constant voltage for 12 h, and setting aside for 30 s. Finally, the system was discharged at 0.1 C constant current to 1.7 V for three times. Then the above cycle was repeated at 0.5 C, 1 C, 0.5 C, and 0.1 C, respectively.

Fig. 1 shows a diagram of the homemade simulated test battery. In particular, Fig. 1a shows the homemade electrode plates used for electrochemical testing, Fig. 1b shows the plates for testing the cycle life and multiplier test of the battery at HRPSoC, both of which are negative plates, and Fig. 1c shows the homemade 2.0 V closed lead-acid battery in the laboratory.

3. Results and discussion

3.1. Characterization of CF

Fig. 2a–d reveals the SEM and EDS images of the CF material. It can be observed that the CF exhibits an interconnected honeycomb-like morphology, indicating a rich porous structure that facilitates electronic transfer and rapid ion diffusion [26]. The AC powder, serving as a foaming agent, contributes to the formation of the honeycomb-like structure and micro-pores within the carbon material. Additionally, during the pyrolysis process, hydrophobic carbon segregates from water, resulting in the presence of macropores and mesopores in the CF material [27]. The EDS energy spectrum shows that the CF material contains two elements, C and O, and both elements are uniformly distributed on the porous spheres. From the total CF spectrum in Fig. 2e, it can be seen that the atomic percentages of C and O are 93.99 % and 6.01 %, respectively.

The Raman spectroscopy technique allows for the measurement of molecular vibrations and rotations, enabling analysis of molecular structure. Fig. 3a presents the Raman comparison of CF and AC, The D band is put down to the vibration of sp^3 hybridized carbon atoms, while the G band corresponds to the in-plane vibration of sp^2 hybridized carbon atoms [28–30]. The degree of disorder and graphitization of a carbon material can be revealed in terms of the strength ratio of the D and G bands (I_D/I_G). A smaller I_D/I_G value
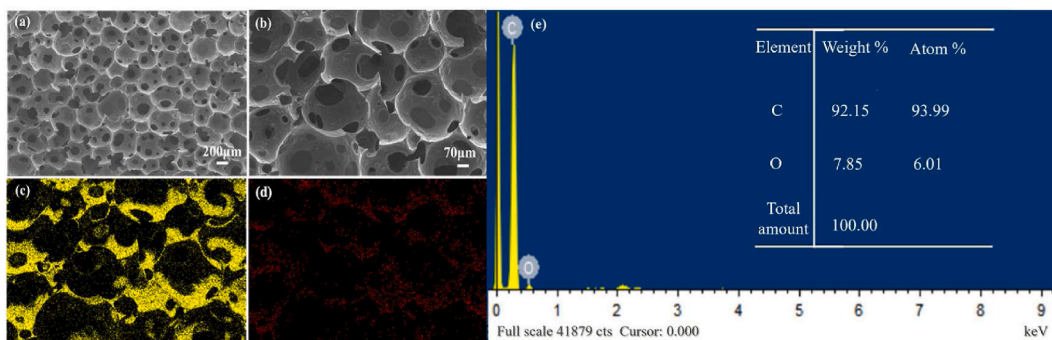

Fig. 1. Homemade simulated test battery.

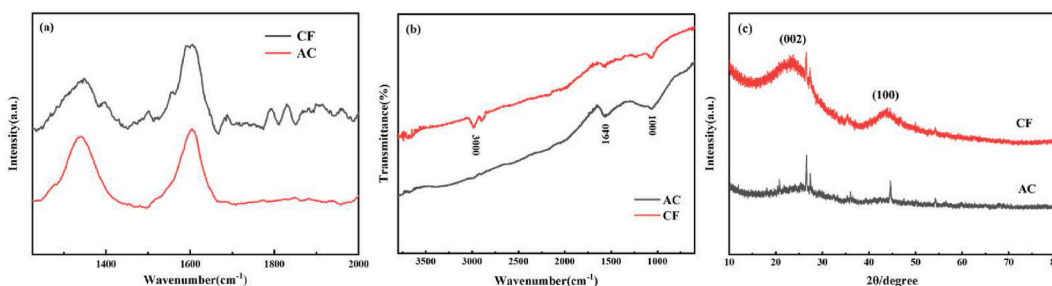**Fig. 2.** (a, b) SEM; (c, d) EDS; (e) Total spectrum of carbon foams.

Fig. 3. (a) Raman; (b) Infrared and (c) XRD spectra of carbon foams.

indicates a higher degree of graphitization in the carbon material [31,32]. The D band at 1350 cm^{-1} of the CF material is related to disordered defects in carbon while the G band at 1581 cm^{-1} is associated with the degree of graphitization [33]. The I_D/I_G of CF (0.406) is lower than that of AC powder (0.931), indicating a higher degree of graphitization of CF. This facilitates the formation of conductive network by CF in NAM and increases the NAM conductivity, thereby enhancing the conversion of Pb/PbSO$_4$.

Fig. 3b shows the FT-IR spectra of AC and CF. The absorption peaks of CF at 2890 cm^{-1} while 3000 cm^{-1} are equal to the C–H stretching vibration of alkanes, the absorption peaks at around 1630 cm^{-1} correspond to the C=O stretching vibration, and the absorption peak at 1100 cm^{-1} is equal to the C–C is the stretching vibration. The absorption peaks of AC at 3420 cm^{-1}, 1640 cm^{-1}, and 1100 cm^{-1} are equal to –OH and C–H vibration, respectively.

The physical phase of the material can be analyzed by XRD measurements and the XRD measurements of CF are shown in Fig. 3c. The two broad diffraction peaks of the sample at around 24° and 43° correspond to the (002) and (100) planes of graphitic carbon, respectively, representing the amorphous character of the carbon material [34,35]. In addition, a weak characteristic diffraction peak of graphitic carbon appeared around 26.2°, suggesting the presence of some graphitic microcrystalline structures in the sample. It is found that the peak of CF (002) is sharper, indicating that the graphitization degree of CF is higher than that of AC [36]. Higher degree
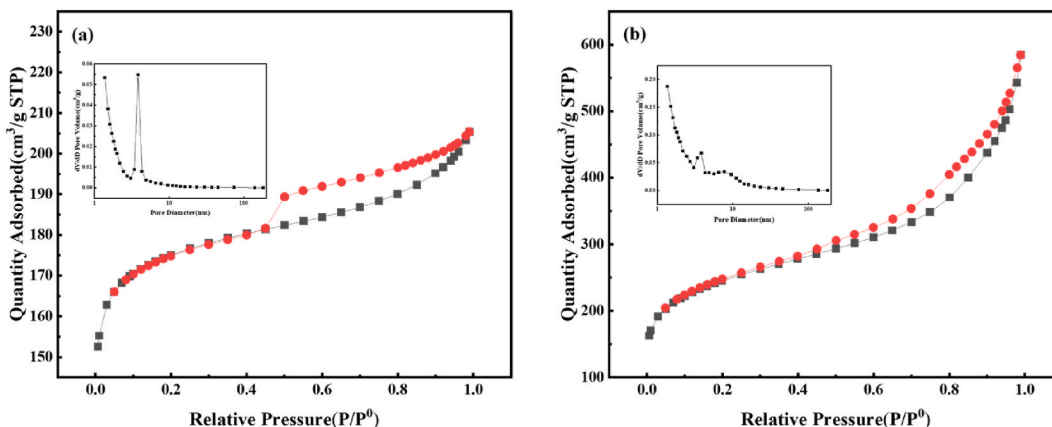

Fig. 4. N$_2$ adsorption-desorption isotherm and pore size distribution: (a) carbon foams; (b) AC.

of graphitization facilitates the formation of conductive network of carbon in the NAM, providing more reactive sites for the electrolyte and promoting the battery charging and discharging efficiency [37].

The N_2 adsorption-desorption isotherm plot and pore size distribution plot were used to analyze the specific surface area of CF. As shown in Fig. 4a, the N_2 adsorption-desorption isotherm of CF exhibits a distinct type IV isotherm, indicating a strong interaction between CF and nitrogen [24]. The CF material is porous as it contains abundant mesopores and micropores. Mesopores serve as the primary sites for electrolyte reactions, and the rich mesoporous structure of CF facilitates sufficient contact between the electrolyte and NAM. The isotherm also exhibits a significant hysteresis loop, representing H4-type narrow slit pores, similar to those generated by layered structures [38,39]. The point of hysteresis line at 0.5 P/P^0 corresponds to the point of 3.8 nm in the pore size distribution diagram, manifesting the influence of mesopores. The BET specific surface area of CF is 538.326 m^2/g, and the larger specific surface area is conducive to the full contact between the electrolyte and the NAM, enhancing the conversion efficiency of Pb and $PbSO_4$. The pore volume of CF is 0.094 cm^3/g, primarily distributed in the range of 0–5 nm. The specific surface area of AC in Fig. 4b is 806.597 m^2/g, and the pore size distribution is between 0 and 20 nm. Table 1 shows the specific surface area and pore size data of CF and AC materials, the average pore size of CF is 3.832 nm, the pore size is between 2 and 50 nm, mainly mesoporous. The average pore size of AC is 1.371 nm, and the pore size is less than 2 nm, mainly microporous. The mesopore of CF material is more conducive to the full reaction between NAM and electrolyte.

The content and distribution of elements in the CF material were analyzed using the XPS technique, and the XPS spectra and C 1s and O 1s spectra of CF are shown in Fig. 5a–c, respectively. The XPS spectrum of the material contains C and O elements, which is consistent with the previous EDS spectra. Fig. 5b shows the C 1s spectrum of the material, where a clear C–C peak can be observed around 285 eV, and two slightly weaker peaks around 286.6 eV and 287.6 eV correspond to C–O and C=O bonding, respectively. The O 1s spectrum of CF also shows three peaks, with the highest peak at 533.1 eV corresponding to the C–O peak, followed by the C=O peak around 531.2 eV, and the weakest peak corresponds to the O=C–O peak of 536 eV.

3.2. Electrochemical analysis

Electrochemical tests, including CV, LSV, and EIS, were conducted to investigate the effect of CF additive on the electrode plate. CV was used to lucubrate the effect of additives on the capacitive performance of the negative electrode plate [40]. The results of the CV measurement are shown in Fig. 6a and b. In the figures, the oxidation peaks in the figure are accordant to the oxidation of Pb to $PbSO_4$, and the reduction peaks conform to the reduction of the formed $PbSO_4$ to spongy Pb [41]. Since the reaction was carried out in a three-electrode system, only the oxidation peak can be observed in the CV plot due to the low accumulation of $PbSO_4$ on the working electrode. Fig. 6a compares the CV plots of the blank group and the same additive amount of AC and CF electrode plates. Compared with the blank group without additives, the oxidation peak of the negative electrode plate with AC addition was somewhat improved, while the negative electrode plate with CF addition had a higher oxidation peak current and a larger peak area, indicating that the negative electrode plate with CF addition had a larger capacity. This is due to the fact that the carbon material can form a conductive network in the NAM, increase the NAM conductivity, and improve the charge/discharge reversibility of the electrode plate, thus effectively inhibiting the sulfation of the negative electrode plate. Fig. 6b shows the CV plots of the electrodes with different additions of CF. With the increase of CF content, the electrochemical performance of the negative electrode plate firstly rises and then decreases, among which the best electrochemical performance is achieved at the additive amount of 1.0 % CF. The electrochemical performance of the electrode plate is continuously improved before the additive amount of CF is 1.0 %, which suggests that the addition of the CF material can effectively alleviate the irreversible sulfation of the negative electrode plate and increase the capacitance performance of the electrode plate. However, when the CF content exceeds 1.0 %, the electrochemical performance of the electrode plate decreases, possibly due to the agglomeration of excessive carbon material in the negative plate, resulting in a deterioration of its electrochemical characteristics.

During the charging process, hydrogen gas is generated on the negative plate, which impacts the internal structure of the plate and leads to structural damage [42]. Excessive hydrogen evolution also leads to increased water loss from the battery and increased electrolyte concentration, affecting the cycle life of the battery. Therefore, LSV testing of the negative plate were performed to analyze the hydrogen evolution. Fig. 6c shows the comparison of hydrogen evolution of the blank group, AC group and the negative plate with CF material added, from which it can be seen that the hydrogen evolution current density of the negative plate with 1.0 % CF added is lower than that of the negative plate with AC added. It may be due to a higher overpotential for hydrogen evolution on the CF-added negative plate compared to the AC-added negative plate. CF has a lower specific surface area than AC, and the relatively high specific surface area of AC provides more hydrogen evolution sites, so AC has a higher hydrogen evolution current density [43]. Fig. 6d shows the LSV plots of negative electrode plates with different CF additions. Compared with the blank group, the hydrogen evolution of the electrode plate with CF addition increased significantly. This is attributed to the low overpotential for hydrogen evolution of carbon materials, and the addition of carbon reduces the overpotential for hydrogen evolution on the electrode surface, leading to an increased hydrogen evolution rate. Table 2 shows the hydrogen evolution current densities of negative electrode plates with CF

Table 1
Specific surface area and pore size analysis of CF and AC materials.

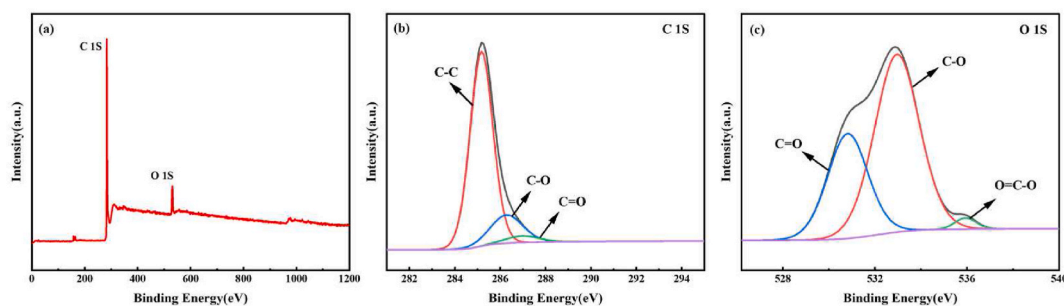| Type	Specific surface area (m^2/g)	Pore volume (cm^3/g)	Average pore diameter (nm)
CF	538.326	0.094	3.832
AC	806.597	0.755	1.371

Fig. 5. (a) Total XPS spectra of carbon foams; (b) C 1s; (c) O 1s spectra.
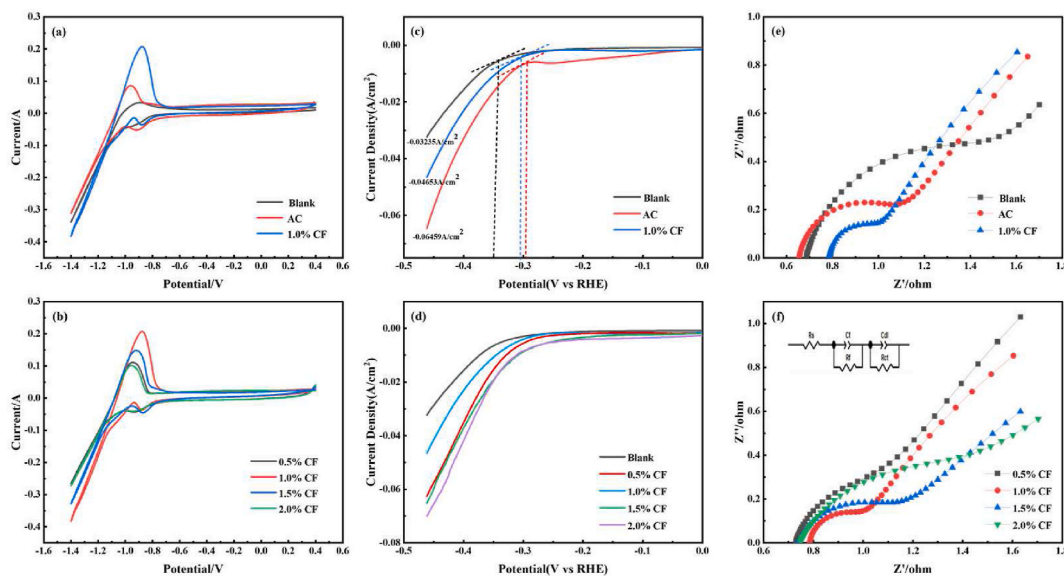

Fig. 6. (a) CV; (c) LSV and (e) Nyquist plots for the blank group, AC group, and 1.0 % carbon foams group; (b) CV; (d) LSV and (f) Nyquist plots and equivalent circuit diagrams for electrode plates with different carbon foams contents.

additions of 0.5 %, 1.0 %, 1.5 %, and 2.0 %, respectively, at the same voltage, where the absolute value of the hydrogen evolution current density of the 1.0 % CF battery is the smallest. The hydrogen evolution current density increased with the increase of carbon content. The hydrogen evolution test results of the electrode plates showed that the negative plate with 1.0 % CF content had the best electrochemical performance, consistent with the CV measurement results.

At open-circuit potential, the lead-carbon electrodes are mainly involved in Pb/PbSO$_4$ interconversion [44]. By testing the EIS at open-circuit potential, the reversible effect of CF material on Pb/PbSO$_4$ interconversion can be characterized. The Nyquist plots and equivalent circuit diagrams obtained using Zview fitting are shown in Fig. 6e and f. R$_s$ in the equivalent circuit diagram represents the resistance and R$_{ct}$ represents the charge transfer resistance, reflecting the charge transfer resistance between the electrode surface and the reactants in the electrolyte [45]. The Nyquist plot consists of an irregular semicircle in the high-frequency region and a straight line in the low-frequency region; the semicircle is related to the charge transfer resistance while the straight line is related to the Z$_w$ impedance [46–48]. The smaller the semicircle and the greater the slope of the line, the lower its resistance [49]. From the figure, it can be seen that the addition of CF in the negative electrode plate can reduce the R$_{ct}$ value significantly effectively lowering the electrode

Table 2
Hydrogen evolution current density with different carbon foams contents.

Battery type	Hydrogen evolution current density (A/cm^2)
Blank	−0.032
0.5 % carbon foams	−0.064
1.0 % carbon foams	−0.046
1.5 % carbon foams	−0.063
2.0 % carbon foams	−0.070

impedance. Among them, the negative plate with 1.0 % CF addition has the smallest R_{ct} value, indicating that this negative plate has the lowest impedance and the highest conversion efficiency between Pb and PbSO$_4$. This is due to the high degree of graphitization of the CF material, allowing it to form a conductive network in the neutral ammonium electrolyte, enhancing the conductivity of the system while providing additional reaction sites for the electrolyte, improving the conversion efficiency between Pb and PbSO$_4$.

3.3. Battery testing and analysis

To investigate the role of CF additive in batteries, performance tests including charge-discharge and cycle life were conducted on simulated batteries. As shown in Fig. 7, the comparison of charge-discharge capabilities of the simulated batteries was analyzed for the blank group, AC group, 0.5 % CF group, 1.0 % CF group, 1.5 % CF group, and 2.0 % CF group. From the charging performance curves of each simulated battery at 0.02A current in Fig. 7a, it can be seen that the batteries in the blank and AC groups polarize fast, the voltage rises faster, and the capacity of the batteries is low compared to the CF batteries. While CF can reduce the charge polarization, reduce the rapid voltage rise during the battery charging process and improve the charging performance of the battery. This may be due to the high active surface area of CF, which leads to the high charge acceptance capacity of the battery [50]. In all the CF-added batteries, the charging performance increases and then decreases with the increase of CF addition, where the 1.0 % CF battery has the lowest charge polarization and the slowest voltage rise. This is due to the fact that the carbon material can be able to form a conductive network in the NAM, which improves the NAM conductivity and reduces the battery polarization [19].

Fig. 7b–d shows the discharge curves of the added CF battery at 0.1C, 0.5C and 1C multiplicities. Under the same discharge current density, the discharge capacity of the CF-added battery is larger than that of both the blank group and the AC group, indicating better charge-discharge performance. With increasing CF content, the discharge capacity of all the groups initially increased and then decreased, reaching the maximum at 1.0 % CF content. In low-current discharge, the discharge capacities of the simulated batteries were close to each other, showing similar discharge performance. As the discharge current density increased, the discharge performance of the battery with added CF was significantly better than that of the blank and AC groups. Specifically, when the discharge current density increased from 0.1C to 1C, the discharge capacity of the blank group and the AC group decreased significantly, while the CF-added battery group still maintained a better discharge capacity. This is because the porous structure of CF can provide excess
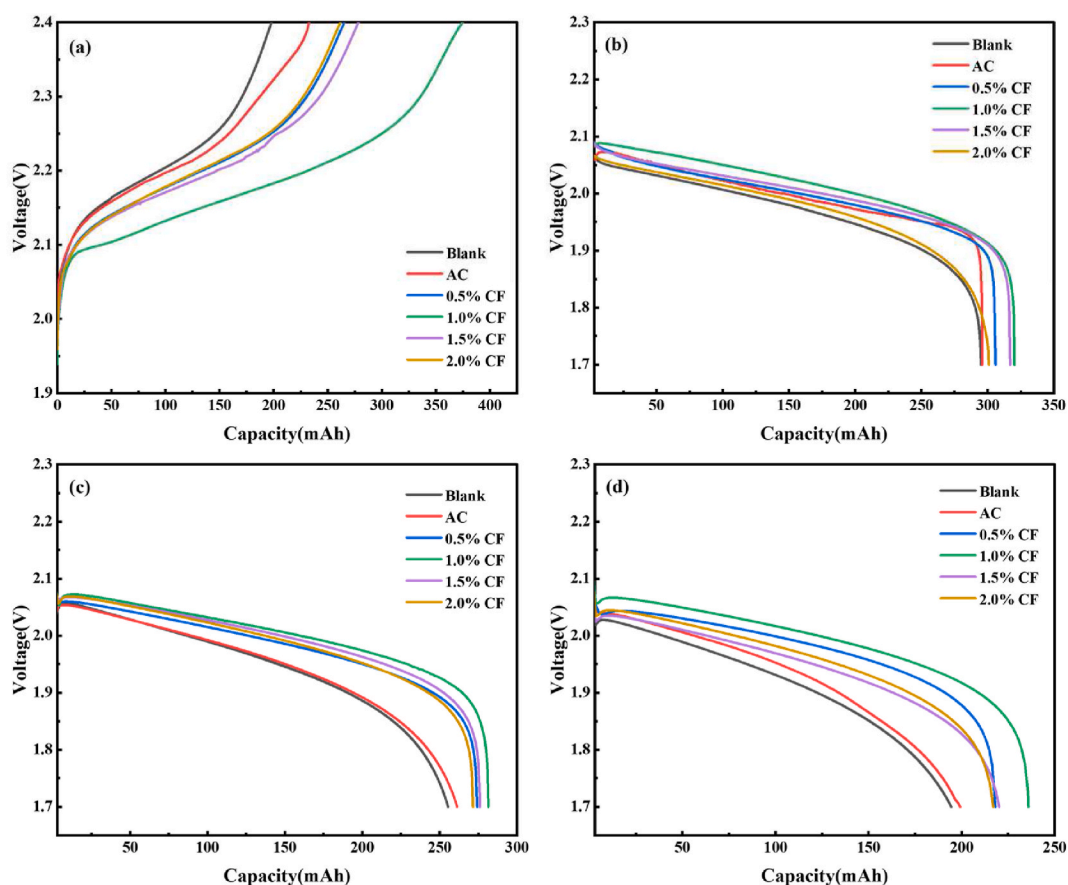

Fig. 7. Charge/discharge performance curves of carbon foams groups (a) charging performance; (b) 0.1C; (c) 0.5C and (d) 1.0C multiplicity discharge performance.

reaction sites and transport channels for the sulfuric acid electrolyte, facilitating the electrolyte to enter the negative electrode plate and make more contact with the neutral aqueous medium. This promotes the conversion of large $PbSO_4$ crystals into sponge-like Pb active materials, improving the utilization of the neutral aqueous medium and thereby enhancing the charge-discharge capabilities of the battery [51].

Fig. 8a shows the cycle life graphs of each simulated battery pack under HRPSoC conditions. The cycle life of the blank group, AC group, 0.5 % CF group, 1.0 % CF group, 1.5 % CF group, and 2.0 % CF group are 1267 cycles, 1521 cycles, 1884 cycles, 3642 cycles, 2077 cycles, and 1803 cycles, respectively, when tested at 2C current density in a 50 % state of charge (SoC). The cycle life of the battery group with added CF material was greatly improved, with the highest cycle life of 1.0 % CF, which was 2.87 times of the blank group and 2.39 times of the AC group. When the amount of CF added is higher than 1.0 %, the cycle life of the battery may gradually decrease due to the agglomeration of carbon materials, but it is still higher than that of the blank and AC groups. This is because the added porous carbon material can provide channels for the electrolyte and promote the interconversion between $Pb/PbSO_4$, thus effectively inhibiting the negative electrode sulfation and improving the battery cycle life [52,53].

To further investigate the effect of CF additives on battery performance, the capacity measurement graphs of each group of batteries at different discharge multiplicities were plotted as shown in Fig. 8b. All the batteries displayed the highest capacity at 0.1C discharge rate, which gradually decreased with increasing discharge rate. From the graph, it can be seen that the discharge capacity of the CF-added batteries is higher than that of the blank and AC groups at any discharge rate. And among the batteries with different CF additions, 1.0 % CF battery has the highest capacity. When the discharge multiplication rate increased, the discharge capacity of the blank and AC groups decreased significantly with the increase of discharge current density, while the CF-added battery group still maintained a high discharge capacity. As the discharge rate increased, the discharge capacity of the blank group and AC group significantly decreased with increasing discharge current density, while the battery groups with CF additives maintained higher discharge capacities. When the discharge rate was reduced to 0.1C again, the CF-added battery experienced less capacity loss compared to the blank group and AC group. The results of the rate test align with the charge-discharge performance test results, indicating that adding CF material to the battery can improve the reversibility of the charging/discharging process, suppress irreversible sulfation at the negative electrode, enhance the utilization of the neutral aqueous medium, and consequently improve the high-rate charge-discharge capabilities of the battery.

3.4. Characterization of batteries before and after cycling

In order to investigate the mechanism of CF additives on the battery, the battery plates before and after cycling were selected for SEM, XRD and other measurements and analyses. The SEM images of the negative plate before and after cycling of the blank group, AC group and the battery with 1.0 % CF addition are shown in Fig. 9, and a large amount of sponge Pb can be observed in the SEM images of each battery group before cycling [54]. The Pb particles aggregated together (Fig. 9a), which is detrimental to the participation of NAM in the electrode reaction and affects the cycle life of the battery. The sponge Pb phase of the negative plates with added carbon materials (Fig. 9c and e) was more dispersed, indicating that the addition of carbon materials to the negative plates can improve the NAM utilization rate and increase the battery cycle life [19,55]. After cycling of each battery group, as shown in Fig. 9b and d, large $PbSO_4$ crystals existed in the negative plates of the blank and AC groups of batteries, which were piled up together and prevented the electrolyte from entering the inside of the plates, resulting in that only a small amount of $PbSO_4$ on the surface could be converted into sponge Pb during charging. The negative electrode plate with added CF (Fig. 9f) has fewer large $PbSO_4$ crystals, smaller $PbSO_4$ crystal size and uniform grain dispersion, which is conducive to the electrolyte entering the electrode plate to participate in the reaction, improving the NAM utilization rate and the $Pb/PbSO_4$ conversion rate, and effectively inhibiting the sulfation of the negative electrode plate.
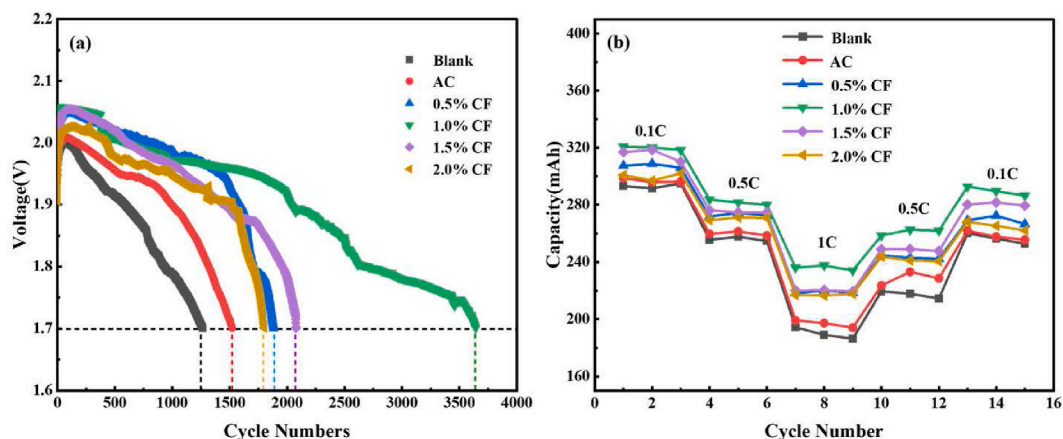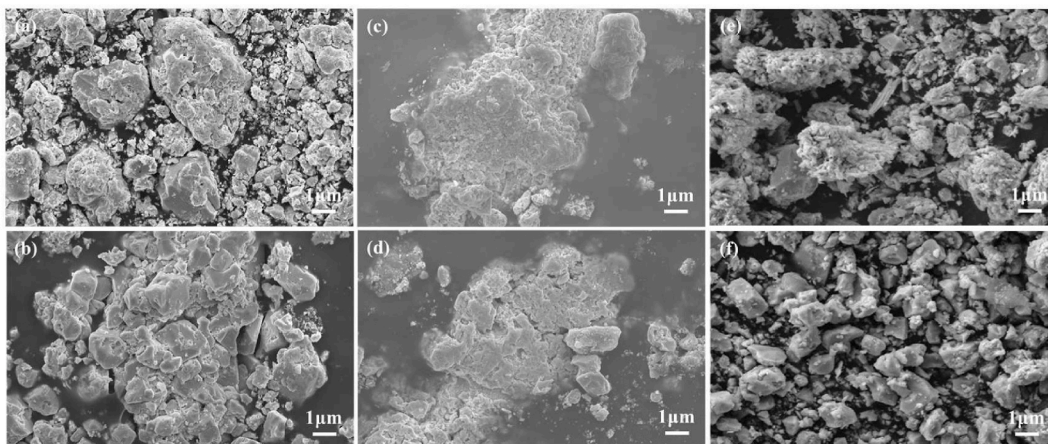

Fig. 8. (a) Cycle life graphs of each batterie groups under HRPSoC at 2C current density; (b) Discharge capacity test at different multiplicities for blank group, AC group and carbon foams groups.

Fig. 9. SEM images of the negative plate groups before HRPSoC cycling: (a) blank group, (c) AC group, and (e) carbon foams groups; SEM images of the negative plate after HRPSoC cycling: (b) blank group, (d) AC group, and (f) carbon foams groups.

Fig. 10a shows the XRD analysis of the simulated batteries after cycling for the blank group, AC group and CF group with different additions. From the figure, it can be seen that a large amount of $PbSO_4$ phase and a small amount of metal Pb phase existed in each battery group after cycling. Facilitating Rietveld quantitative analysis with HighScore Plus software, the content of $PbSO_4$ phase was 88.9 %, 73.2 %, 66.6 %, 52.8 %, 59.2 %, and 69.1 % in the blank, AC, 0.5 % CF, 1.0 % CF, 1.5 % CF, and 2.0 % CF groups, respectively. Compared to the blank and AC groups, the CF-added battery groups exhibit a lower content of $PbSO_4$ phase, with 1.0 % CF showing the least amount of $PbSO_4$ phase. This indicates that the addition of CF material can effectively prevent the accumulation of large-size $PbSO_4$ crystals and inhibit the sulfation of the negative plate. Three strong $PbSO_4$ peaks with $2\theta = 26.71°$, $29.68°$ and $43.76°$ in the XRD plots were selected to compare their half peak widths. The grain size of $PbSO_4$ can be calculated by applying Debye-Scherrer formula [56]: $D = K\lambda/(\beta \cos \theta)$. where D represents the grain size; K is Scherrer's constant; λ is the X-ray wavelength, which is generally taken as 1.54056 Å for Cu kα; β is the half-height width of the diffraction peak; and θ is the Bragg diffraction angle. From the formula, it can be seen that the half-height width has an inverse relationship with the grain size, and the smaller the half-height width value is, the larger the grain size is. As can be seen from Fig. 10b, compared with the blank and AC groups, the battery groups with CF have higher half peak width values and smaller grain sizes, which is consistent with the previous SEM structure. It indicates that the addition of CF material can reduce the size of $PbSO_4$ crystals and prevent the large accumulation of $PbSO_4$, thus inhibiting the sulfation of the negative plate. The half-peak width value of the battery with CF addition is larger than that of the AC group, indicating that the CF material has a stronger ability to suppress sulfation than AC. And among the different CF additions, the 1.0 % CF battery has the smallest $PbSO_4$ grain size and the best sulfation inhibition effect, which is consistent with the XRD test results. This indicates that adding an appropriate amount of CF can effectively inhibit the formation and aggregation of irreversible $PbSO_4$, thus improving the battery's charge/discharge performance and cycle life.

3.5. Mechanism of CF in lead-acid batteries

Based on the comprehensive analysis of the above tests, the mechanism of CF material in the negative plate of lead-acid batteries can be inferred. Fig. 11 shows the mechanism of the negative plate without carbon material and with CF at HRPSoC. In the blank group without added carbon material, large $PbSO_4$ crystals were generated on the surface of the negative plate after high-rate discharge, and it was difficult for these large $PbSO_4$ crystals to be completely converted into sponge Pb [57–59]. The accumulation of $PbSO_4$ formed an insulating layer, which prevented the electrolyte from entering into the interior of the negative plate, leading to the reduction of the utilization rate of NAM, and the decrease of the battery capacity and the cycling performance. The CF material can provide additional reaction sites for H_2SO_4, which is easy to generate small-sized $PbSO_4$ crystals, and these small-sized crystals are more easily and uniformly dispersed throughout the plate, preventing the formation of a dense $PbSO_4$ insulating layer, which is conducive to the electrolyte entering the interior of the negative plate and reacting with the NAM, and improving the electrochemical performance of the battery. In addition, the porous structure of CF can form a conductive network in the negative electrode plate and increase the NAM conductivity, thus improving the $Pb/PbSO_4$ conversion efficiency and increasing the battery cycle life [60,61].

4. Conclusions

In this study, we prepared a porous CF material by using AC foam method, and then investigated its electrochemical properties through CV, LSV, and EIS tests. We added the CF material to the negative plate to assemble batteries for performance analysis. CF possessed a layered porous carbon structure and contained carbon and oxygen elements. The graphitization degree of CF was higher than that of AC, making it more favorable for CF to form a conductive network in NAM and enhance the electrochemical performance of the negative plate. The pores of CF were mainly composed of micropores and mesopores, with mesopores being the primary reaction
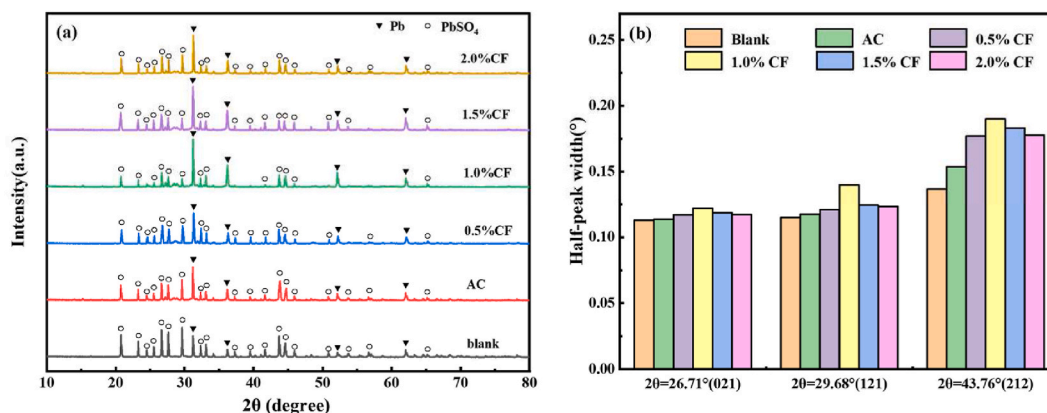
Fig. 10. (a) XRD (b) $PbSO_4$ half-peak widths of blank group, AC group, and carbon foams groups after HRPSoC cycling.
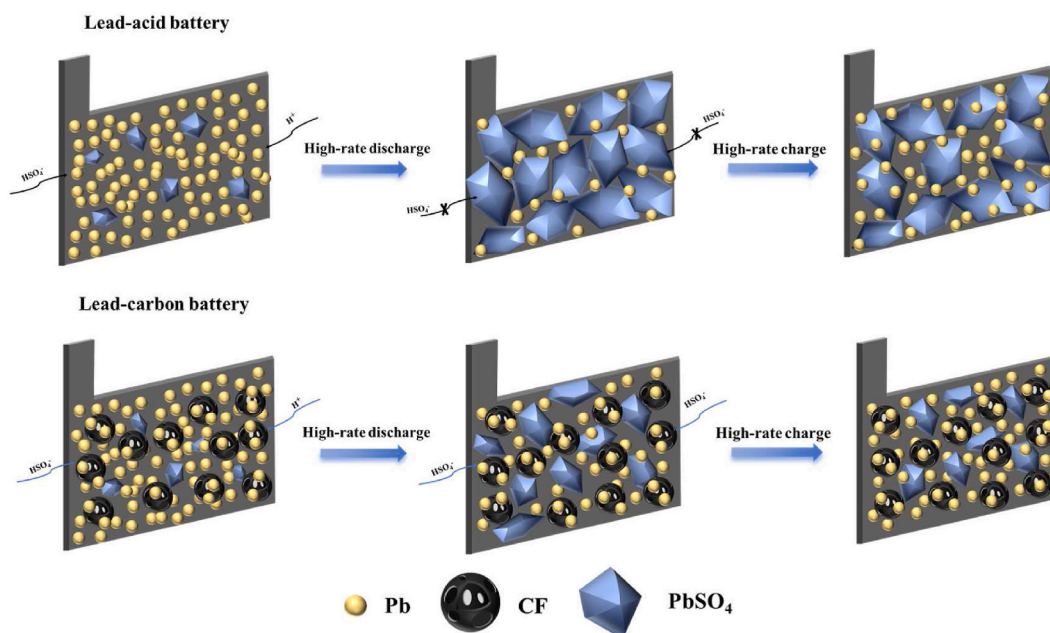

Fig. 11. Mechanism of carbon foams in the negative plate of lead-acid batteries.

sites for the electrolyte. Therefore, the addition of CF material facilitated the full reaction between the electrolyte and NAM. Electrochemical tests revealed that the addition of CF increased the capacity and improved the electrochemical performance of the negative plate. Furthermore, CF addition increased the conductivity of NAM and reduced the impedance of the plate. When the CF addition amount was 1.0 %, the negative plate showed the highest capacity and the lowest impedance, exhibiting the best electrochemical performance. Assembled into sealed batteries, the negative plates with CF showed significantly improved charge/discharge capacity, and the cycle life of the CF-added battery under HRPSoC was 2.87 times higher than that of the blank group. Additionally, the CF-added battery maintained high capacity even under high-rate discharge conditions. The battery with 1.0 % CF exhibited the best performance, and further increase in CF content may lead to a decrease in battery performance due to CF aggregation. The $PbSO_4$ crystals in the negative plates after cycling were smaller and more dispersed than those in the blank and AC groups, indicating higher NAM utilization and effective prevention of irreversible sulfate formation on the negative plate. This improved the charge/discharge performance and cycle life of the battery.

CF materials prepared by sucrose-based foaming are green, inexpensive and simple to prepare, and better electrochemical performance and cycle life than AC were obtained in the experimental stage. However, due to the small laboratory preparation simulation battery and the difference between the laboratory process and the production plant, the carbon materials still have shortcomings in practical applications. For example, the current can be uniformly distributed during the test of the experimental simulated battery, but the lead-acid battery in the actual production is large in size, and the current cannot be uniformly distributed in the electrode plates during charging and discharging, which leads to a smaller cycle life than that of the experimental simulated battery. In addition, the

difference between the density of lead and carbon is large, and it is difficult to mix the two evenly, which is easy to cause the electrode plate floating carbon. As well as the low hydrogen evolution overpotential of carbon, it is easy to cause water loss in the battery. Therefore, the current research should focus on finding composite materials that can solve the problem of poor compatibility between lead and carbon and inhibit hydrogen evolution, which will be of great significance for the practical application of carbon materials.

Data availability statement

The data presented in this study are available in the article.

CRediT authorship contribution statement

Fazhi Xie: Writing – review & editing, Validation, Supervision, Funding acquisition, Conceptualization. **Yujia Ma:** Writing – original draft, Validation, Methodology, Investigation, Data curation. **Meng Zhang:** Software, Methodology, Investigation. **Shaohua Yang:** Resources, Project administration. **Yuan Dai:** Writing – review & editing, Investigation. **Liang Fang:** Resources, Investigation. **Yonggang Shao:** Validation, Resources.

Declaration of competing interest

The authors declare the following financial interests/personal relationships which may be considered as potential competing interests:

Fazhi Xie reports financial support was provided by National Natural Science Foundation of China. Fazhi Xie reports financial support was provided by National Key Research and Development Program of China. Fazhi Xie reports financial support was provided by the University Synergy Innovation Program of Anhui Province. If there are other authors, they declare that they have no known competing financial interests or personal relationships that could have appeared to influence the work reported in this paper.

References

[1] F. Cheng, J. Liang, Z. Tao, J. Chen, Functional materials for rechargeable batteries, Adv. Mater. 23 (15) (2011) 1695–1715, https://doi.org/10.1002/adma.201003587.
[2] Y. Chang, X. Mao, Y. Zhao, S. Feng, H. Chen, D. Finlow, Lead-acid battery use in the development of renewable energy systems in China, J. Power Sources 191 (1) (2009) 176–183, https://doi.org/10.1016/j.jpowsour.2009.02.030.
[3] P.P. Lopes, V.R. Stamenkovic, Past, present, and future of lead-acid batteries, Science 369 (6506) (2020) 923–924, https://doi.org/10.1126/science.abd3352.
[4] O. Jhabli, M. Boutamart, S. Rafqah, Y. Redouany, A. Bouhmmad, K. Nouneh, S. Briche, The evolution tracking of tribasic lead sulfates features in lead-acid battery positive electrode using design of experiments, J. Electrochem. Soc. 169 (11) (2022) 110501, https://doi.org/10.1149/1945-7111/ac992f.
[5] Y. Zhang, C. Zhou, J. Yang, S. Xue, H. Gao, X. Yan, Q. Huo, S. Wang, Y. Cao, J. Yan, Advances and challenges in improvement of the electrochemical performance for lead-acid batteries: a comprehensive review, J. Power Sources 520 (2022) 230800, https://doi.org/10.1016/j.jpowsour.2021.230800.
[6] D. Pavlov, V. Naidenov, Y. Milusheva, S. Vassilev, T. Shibahara, M. Tozuka, Benzyl benzoate as an inhibitor of the sulfation of negative electrodes in lead-acid batteries, J. Energy Storage 17 (2018) 336–344, https://doi.org/10.1016/j.est.2018.03.021.
[7] M. Shiomi, T. Funato, K. Nakamura, K. Takahashi, M. Tsubota, Effects of carbon in negative plates on cycle-life performance of valve-regulated lead/acid batteries, J. Power Sources 64 (1–2) (1997) 147–152, https://doi.org/10.1016/S0378-7753(96)02515-3.
[8] D. Pavlov, P. Nikolov, Capacitive carbon and electrochemical lead electrode systems at the negative plates of lead-acid batteries and elementary processes on cycling, J. Power Sources 242 (2013) 380–399, https://doi.org/10.1016/j.jpowsour.2013.05.065.
[9] H. Dietz, J. Garche, K. Wiesener, On the behaviour of carbon black in positive lead-acid battery electrodes, J. Appl. Electrochem. 17 (1987) 473–479, https://doi.org/10.1007/BF01084120.
[10] M. Calábek, K. Micka, P. Křivák, P. Bača, Significance of carbon additive in negative lead-acid battery electrodes, J. Power Sources 158 (2) (2006) 864–867, https://doi.org/10.1016/j.jpowsour.2005.11.022.
[11] C. Shen, C. Feng, N. Zhang, B. Yang, L. Su, L. Wang, Hierarchical porous carbon material regenerated from natural bamboo-leaf: how to improve the performance of lead-carbon batteries, J. Power Sources 516 (2021) 230664, https://doi.org/10.1016/j.jpowsour.2021.230664.
[12] A. Banerjee, B. Ziv, Y. Shilina, E. Levi, S. Luski, D. Aurbach, Single-wall carbon nanotube doping in lead-acid batteries: a new horizon, ACS Appl. Mater. Interfaces 9 (4) (2017) 3634–3643, https://doi.org/10.1021/acsami.6b13377.
[13] P. Lee, J. Lee, H. Lee, J. Yeo, S. Hong, K.H. Nam, D. Lee, S.S. Lee, S.H. Ko, Highly stretchable and highly conductive metal electrode by very long metal nanowire percolation network, Adv. Mater. 24 (25) (2012) 3326–3332, https://doi.org/10.1002/adma.201200359.
[14] M. Saravanan, M. Ganesan, S. Ambalavanan, An in situ generated carbon as integrated conductive additive for hierarchical negative plate of lead-acid battery, J. Power Sources 251 (2014) 20–29, https://doi.org/10.1016/j.jpowsour.2013.10.143.
[15] X. Li, Y. Zhang, Z. Su, Y. Zhao, X. Zhao, R. Wang, Graphene nanosheets as backbones to build a 3D conductive network for negative active materials of lead-acid batteries, J. Appl. Electrochem. 47 (2017) 619–630, https://doi.org/10.1007/s10800-017-1067-0.
[16] Q. Long, G. Ma, Q. Xu, C. Ma, J. Nan, A. Li, H. Chen, Improving the cycle life of lead-acid batteries using three-dimensional reduced graphene oxide under the high-rate partial-state-of-charge condition, J. Power Sources 343 (2017) 188–196, https://doi.org/10.1016/j.jpowsour.2017.01.056.
[17] S.W. Swogger, P. Everill, D.P. Dubey, N. Sugumaran, Discrete carbon nanotubes increase lead acid battery charge acceptance and performance, J. Power Sources 261 (2014) 55–63, https://doi.org/10.1016/j.jpowsour.2014.03.049.
[18] D. Pavlov, T. Rogachev, P. Nikolov, G. Petkova, Mechanism of action of electrochemically active carbons on the processes that take place at the negative plates of lead-acid batteries, J. Power Sources 191 (1) (2009) 58–75, https://doi.org/10.1016/j.jpowsour.2008.11.056.

[19] X. Zou, Z. Kang, D. Shu, Y. Liao, Y. Gong, C. He, J. Hao, Y. Zhong, Effects of carbon additives on the performance of negative electrode of lead-carbon battery, Electrochim. Acta 151 (2015) 89–98, https://doi.org/10.1016/j.electacta.2014.11.027.

[20] J. Xiang, P. Ding, H. Zhang, X. Wu, J. Chen, Y. Yang, Beneficial effects of activated carbon additives on the performance of negative lead-acid battery electrode for high-rate partial-state-of-charge operation, J. Power Sources 241 (2013) 150–158, https://doi.org/10.1016/j.jpowsour.2013.04.106.

[21] O. Jhabli, M. Boutamart, J. Bouziad, A. Ghadbane, S. Rafqah, Y. Redouany, A. Bouhmad, K. Nouneh, M. Galai, R. Hsissou, S. Briche, New insights into carbonaceous materials and lead/carbon composites in lead carbon battery, J. Energy Storage 56 (2022) 106019, https://doi.org/10.1016/j.est.2022.106019.

[22] P.T. Moseley, Consequences of including carbon in the negative plates of Valve-regulated Lead-Acid batteries exposed to high-rate partial-state-of-charge operation, J. Power Sources 191 (1) (2009) 134–138, https://doi.org/10.1016/j.jpowsour.2008.08.084.

[23] A. Jaiswal, S.C. Chalasani, The role of carbon in the negative plate of the lead-acid battery, J. Energy Storage 1 (2015) 15–21, https://doi.org/10.1016/j.est.2015.05.002.

[24] R. Narasimman, Sujith Vijayan, K. Prabhakaran, Carbon particle induced foaming of molten sucrose for the preparation of carbon foams, Mater. Sci. Eng., B 189 (2014) 82–89, https://doi.org/10.1016/j.mseb.2014.08.007.

[25] N. Sudhan, K. Subramani, M. Karnan, N. Ilayaraja, M. Sathish, Biomass-derived activated porous carbon from rice straw for a high-energy symmetric supercapacitor in aqueous and non-aqueous electrolytes, Energy Fuels 31 (1) (2017) 977–985, https://doi.org/10.1021/acs.energyfuels.6b01829.

[26] W. Tian, H. Zhang, X. Duan, H. Sun, G. Shao, S. Wang, Porous carbons: structure-oriented design and versatile applications, Adv. Funct. Mater. 30 (17) (2020) 1909265, https://doi.org/10.1002/adfm.201909265.

[27] L. Qie, W. Chen, H. Xua, X. Xiong, Y. Jiang, F. Zou, X. Hu, Y. Xin, Z. Zhang, Y. Huang, Synthesis of functionalized 3D hierarchical porous carbon for high-performance supercapacitors, Energ Environ. Sci. 6 (8) (2013) 2497–2504, https://doi.org/10.1039/C3EE41638K.

[28] M. Bhar, U. Bhattacharjee, D. Sarma, S. Krishnamurthy, K. Yalamanchili, A. Mahata, S.K. Martha, A novel and sustainable approach to enhance the Li-ion storage capability of recycled graphite anode from spent lithium-ion batteries, ACS Appl. Mater. Interfaces 15 (22) (2023) 26606–26618, https://doi.org/10.1021/acsami.3c02272.

[29] Y. Zhang, M. Chu, L. Yang, Y. Tan, W. Deng, M. Ma, X. Su, Q. Xie, Three-dimensional graphene networks as a new substrate for immobilization of laccase and dopamine and its application in glucose/O_2 biofuel cell, ACS Appl. Mater. Interfaces 6 (15) (2014) 12808–12814, https://doi.org/10.1021/am502791h.

[30] N.V. Qui, P. Scholz, T. Krech, T.F. Keller, K. Pollok, B. Ondruschka, Multiwalled carbon nanotubes oxidized by UV/H_2O_2 as catalyst for oxidative dehydrogenation of ethylbenzene, Catal. Commun. 12 (6) (2011) 464–469, https://doi.org/10.1016/j.catcom.2010.11.007.

[31] L. Wu, J. Cao, Y. Rao, Y. Yang, S. Zhou, Z. Chen, Ash-free porous carbon as the negative additive of lead-acid batteries and supercapacitors, Energy Technol. 11 (4) (2023) 2201394, https://doi.org/10.1002/ente.202201394.

[32] X. Gao, C. Zhan, X. Yu, Q. Liang, R. Lv, G. Gai, W. Shen, F. Kang, Z.H. Huang, A high performance lithium-ion capacitor with both electrodes prepared from Sri Lanka graphite ore, Materials 10 (4) (2017) 414, https://doi.org/10.3390/ma10040414.

[33] H. Hu, N. Xie, C. Wang, L. Wang, R.M. Privette, H. Li, M. Pan, F. Wu, X. Yan, B. Jiang, M.H. Wu, K. Vinodgopal, G. Dai, Enhanced performance of E-bike motive power lead-acid batteries with graphene as an additive to the active mass, ACS Omega 3 (6) (2018) 7096–7105, https://doi.org/10.1021/acsomega.8b00353.

[34] D.H. Jurcakova, M. Kodama, S. Shiraishi, H. Hatori, Z. Zhu, G. Lu, Nitrogen-enriched nonporous carbon electrodes with extraordinary supercapacitance, Adv. Funct. Mater. 19 (11) (2009) 1800–1809, https://doi.org/10.1002/adfm.200801100.

[35] F. Shen, J. Liu, D. Wu, Y. Dong, Z. Zhang, Development of O_2 and NO co-doped porous carbon as a high-capacity mercury sorbent, Environ. Sci. Technol. 53 (3) (2019) 1725–1731, https://doi.org/10.1021/acs.est.8b05777.

[36] W. Deng, T. Li, H. Li, X. Liu, A. Dang, Y. Liu, H. Wu, Controllable graphitization degree of carbon foam bulk toward electromagnetic wave attenuation loss behavior, J. Colloid Interface Sci. 618 (2022) 129–140, https://doi.org/10.1016/j.jcis.2022.03.071.

[37] X. Li, L. Zhang, G. He, Fe_3O_4 doped double-shelled hollow carbon spheres with hierarchical pore network for durable high-performance supercapacitor, Carbon 99 (2016) 514–522, https://doi.org/10.1016/j.carbon.2015.12.076.

[38] K. Yu, Z. Zhang, J. Liang, C. Liang, Natural biomass-derived porous carbons from buckwheat hulls used as anode for lithium-ion batteries, Diamond Relat. Mater. 119 (2021) 108553, https://doi.org/10.1016/j.diamond.2021.108553.

[39] J. Serafin, U. Narkiewicz, A.W. Morawski, R.J. Wróbel, B. Michalkiewicz, Highly microporous activated carbons from biomass for CO_2 capture and effective micropores at different conditions, J. CO_2 Util. 18 (2017) 73–79, https://doi.org/10.1016/j.jcou.2017.01.006.

[40] M. Zhang, H. Song, Y. Ma, S. Yang, F. Xie, Preparation of NH_4Cl-modified carbon materials via high-temperature calcination and their application in the negative electrode of lead-carbon batteries, Molecules 28 (14) (2023) 5618, https://doi.org/10.3390/molecules28145618.

[41] A. Daoud, A.Y. Shenouda, M.T. Abou El-Khair, F. Fairouz, E. Mohamed, M.A. Aziz, k. Yanamandra, N. Gupta, Electrochemical performance of novel Pb alloys reinforced with Ni-coated fly ash microballoon composite foams in Lead Acid Battery, Mater. Chem. Phys. 294 (2023) 126987, https://doi.org/10.1016/j.matchemphys.2022.126987.

[42] L. Zhao, B. Chen, D. Wang, Effects of electrochemically active carbon and indium (III) oxide in negative plates on cycle performance of valve-regulated lead-acid batteries during high-rate partial-state-of-charge operation, J. Power Sources 231 (2013) 34–38, https://doi.org/10.1016/j.jpowsour.2012.12.083.

[43] B. Hong, L. Jiang, H. Xue, F. Liu, M. Jia, J. Li, Y. Liu, Characterization of nano-lead-doped active carbon and its application in lead-acid battery, J. Power Sources 270 (2014) 332–341, https://doi.org/10.1016/j.jpowsour.2014.07.145.

[44] J. Zhong, J. Gu, X. Wang, S. Wang, Quasi-solid synthesis of nano-Pb/C composites for enhanced performance of lead-acid battery, J. Energy Storage 47 (2022) 103535, https://doi.org/10.1016/j.est.2021.103535.

[45] Z. Zhou, W. Li, Z. Fu, X. Xiang, Carbon nanotube-supported Pt-HxMoO3 as electrocatalyst for methanol oxidation, Int. J. Hydrogen Energ 35 (3) (2010) 936–941, https://doi.org/10.1016/j.ijhydene.2009.11.038.

[46] S. Arun, K.U.V. Kiran, S.M. Kumar, M. Karnan, M. Sathish, S. Mayavan, Effect of orange peel derived activated carbon as a negative additive for lead-acid battery under high rate discharge condition, J. Energy Storage 34 (2021) 102225, https://doi.org/10.1016/j.est.2020.102225.

[47] L. Zhang, L. Zuo, W. Fan, T. Liu, NiCo2S4 Nanosheets grown on 3D networks of nitrogen-doped graphene/carbon nanotubes: advanced anode materials for lithium-ion batteries, Chemelectrochem 3 (9) (2016) 1384–1391, https://doi.org/10.1002/celc.201600183.

[48] M. Chen, C. Du, B. Song, K. Xiong, G. Yin, P. Zuo, X. Cheng, High-performance LiFePO4 cathode material from FePO4 microspheres with carbon nanotube networks embedded for lithium ion batteries, J. Power Sources 223 (2013) 100–106, https://doi.org/10.1016/j.jpowsour.2012.09.040.

[49] Q. Cheng, J. Tang, J. Ma, H. Zhang, N. Shinya, L.C. Qin, Graphene and carbon nanotube composite electrodes for supercapacitors with ultra-high energy density, Phys. Chem. Chem. Phys. 13 (39) (2011) 17615–17624, https://doi.org/10.1039/C1CP21910C.

[50] T. Sadhasivam, M.J. Park, J.Y. Shim, J.E. Jin, S.C. Kim, M.D. Kurkuri, S.H. Roh, H.Y. Jung, High charge acceptance through interface reaction on carbon coated negative electrode for advanced lead-carbon battery system, Electrochim. Acta 295 (2019) 367–375, https://doi.org/10.1016/j.electacta.2018.10.149.

[51] Y. Zhang, A. Ali, J. Li, J. Xie, P. Shen, Stereotaxically constructed graphene/nano lead composite for enhanced cycling performance of lead-acid batteries, J. Energy Storage 35 (2021) 102192, https://doi.org/10.1016/j.est.2020.102192.

[52] D. Wang, F. Li, M. Liu, G. Lu, H. Cheng, 3D aperiodic hierarchical porous graphitic carbon material for high-rate electrochemical capacitive energy storage, Angew. Chem. 120 (2) (2008) 379–382, https://doi.org/10.1002/ange.200702721.

[53] W. Zhang, J. Xu, D. Hou, J. Yin, D. Liu, Y. He, H. Lin, Hierarchical porous carbon prepared from biomass through a facile method for supercapacitor applications, J. Colloid Interface Sci. 530 (2018) 338–344, https://doi.org/10.1016/j.jcis.2018.06.076.

[54] J. Gu, J. Zhong, X. Wang, S. Wang, In-situ synthesis of novel nanostructured Pb@ C composites for improving the performance of lead-acid batteries under high-rate partial-state-of-charge operation, J. Energy Storage 33 (2021) 102082, https://doi.org/10.1016/j.est.2020.102082.

[55] S. Zhang, H. Zhang, W. Xue, J. Cheng, W. Zhang, G. Cao, H. Zhao, Y. Yang, A layered-carbon/PbSO4 composite as a new additive for negative active material of lead-acid batteries, Electrochim. Acta 290 (2018) 46–54, https://doi.org/10.1016/j.electacta.2018.08.090.

[56] U. Holzwarth, N. Gibson, The Scherrer equation versus the 'Debye-Scherrer equation', Nat. Nanotechnol. 6 (9) (2011) 534, https://doi.org/10.1038/nnano.2011.145.

[57] F. Yang, H. Zhou, J. Hu, S. Ji, C. Lai, H. Wang, J. Sun, L. Lei, Thorn-like and dendrite lead sulfate as negative electrode materials for enhancing the cycle performance of lead-acid batteries, J. Energy Storage 49 (2022) 104112, https://doi.org/10.1016/j.est.2022.104112.

[58] Y. Yang, J. Cao, X. Liu, W. Huang, S. Zhou, L. Chen, Y. Rao, Z. Chen, L. Wu, Rapid preparation of new carbon materials from pure six-carbon alkane and their use as a negative electrode additive for lead-carbon Batteries, Energy Technol. (2023), https://doi.org/10.1002/ente.202300038.

[59] P. He, J. Tu, Y. Yang, H. Huang, B. Chen, C. Gao, Y. He, Z. Guo, Hierarchical tubular porous carbon derived from mulberry branches for long-life lead-carbon battery, J. Energy Storage 64 (2023) 107162, https://doi.org/10.1016/j.est.2023.107162.

[60] M. Saravanan, P. Sennu, M. Ganesan, S. Ambalavanan, Multi-walled carbon nanotubes percolation network enhanced the performance of negative electrode for lead-acid battery, J. Electrochem. Soc. 160 (1) (2012) A70, https://doi.org/10.1149/2.062301jes.

[61] J. Wang, L. Shen, P. Nie, X. Yun, Y. Xu, H. Dou, X. Zhang, N-doped carbon foam based three-dimensional electrode architectures and asymmetric supercapacitors, J. Mater. Chem. A 3 (6) (2015) 2853–2860, https://doi.org/10.1039/C4TA05932H.